HHS Public Access

Author manuscript

Ann Neurol. Author manuscript; available in PMC 2020 May 09.

Published in final edited form as:

Ann Neurol. 2019 December ; 86(6): 885–898. doi:10.1002/ana.25610.

T-lymphocytes and Cytotoxic Astrocyte Blebs Correlate Across Autism Brains

Marcello M. DiStasio, MD, PhD[1], **Ikue Nagakura, PhD**[1], **Monica J. Nadler, PhD**[1], **Matthew P. Anderson, MD, PhD**[‡,1,2,3]

[1]Departments of Neurology and Pathology, Beth Israel Deaconess Medical Center, 330 Brookline Avenue, Boston, MA 02115, USA.

[2]Boston Children's Hospital Intellectual and Developmental Disabilities Research Center, 300 Longwood Avenue, Boston, MA 02115, USA.

[3]Program in Neuroscience, Harvard Medical School, 300 Longwood Avenue, Boston, MA 02115, USA.

Abstract

Objective—Autism spectrum disorder (ASD) affects 1 in 59 children yet, except for rare genetic causes, the etiology in most ASD remains unknown. In the ASD brain, inflammatory cytokine and transcript profiling show increased expression of genes encoding mediators of the innate immune response. We evaluated post-mortem brain tissue for adaptive immune cells and immune cell-mediated cytotoxic damage that could drive this innate immune response in the ASD brain.

Methods—Standard neuropathology diagnostic methods including histology and immunohistochemistry were extended with automated image segmentation to quantify identified pathologic features in the postmortem brains.

Results—We report multifocal perivascular lymphocytic cuffs contain increased numbers of lymphocytes in ~65% of ASD compared to control brains in males and females, across all ages, in most brain regions, and in white and grey matter, and leptomeninges. $CD3^+$ T-lymphocytes predominate over $CD20^+$ B-lymphocytes and $CD8^+$ over $CD4^+$ T-lymphocytes in ASD brains. Importantly, the perivascular cuff lymphocytes numbers correlate to the quantity of astrocyte-derived round membranous blebs. Membranous blebs form as a cytotoxic reaction to lymphocyte attack. Consistent with multifocal immune cell-mediated injury at perivascular CSF-brain barriers, a subset of white matter vessels have increased perivascular space (with jagged contours) and collagen in ASD compared to control brains. CSF-brain barrier pathology is also evident at cerebral cortex pial and ventricular ependymal surfaces in ASD.

[‡]To whom correspondence should be addressed. Contact: Matthew P. Anderson, MD, PhD, Associate Professor of Pathology, Harvard Medical School, Director of Neuropathology, Department of Pathology, Beth Israel Deaconess Medical Center Faculty, Program in Neuroscience, Harvard Medical School, Investigator, Boston Children's Hospital Intellectual and Developmental Disabilities Research Center, Center for Life Science, 330 Brookline Ave, E/CLS-645, Boston, MA 02215, Tel: (617) 735-3202, FAX: (617) 735-3249, Matthew Anderson@bidmc.harvard.edu.

Author Contributions: M.M.D. and M.P.A. contributed to the conception and design of the study; M.M.D., I.N., and M.J.N. and M.P.A. contributed to the acquisition and analysis of data; M.M.D. and M.P.A. contributed to drafting the text and preparing the figures.

Potential Conflicts of Interest: Nothing to report.

Interpretation—The findings suggest dysregulated cellular immunity damages astrocytes at foci along the CSF-brain barrier in ASD.

Introduction

Autism spectrum disorder (ASD) manifests in early childhood and is diagnosed based on behavioral deficits including impaired social and increased repetitive behaviors and restricted interests. The study of ASD postmortem brain tissue provides insights into the pathologic processes that underlie this disorder currently defined exclusively by behavioral deficits. Using ASD human postmortem brain tissues, investigators have discovered an increase of cytokines, chemokines, growth factors, and activated astroglia and microglia in the cerebral cortex, white matter, and cerebellum in ASD indicating ongoing activity of the innate immune system[1-5]. Genome-wide transcriptional profiling has revealed an increase in the expression of a diverse array of genes encoding mediators of this activated innate immune response along with an overall decrease in the expression of many neuron-related genes[6-8]. Here we applied computer vision algorithms to quantify astrocyte-derived round membranous blebs, multifocal perivascular lymphocytic cuffs, and increased perivascular space and collagen; novel neuropathologic features that we found in a large proportion of ASD brains. The results provide the signatures of a cellular immune response, reflected by T-lymphocyte infiltrates and cytotoxic cell injuries (typical of T-lymphocytes) to CSF-brain barrier astrocytes, in ASD compared to control postmortem brains.

Methods

Study subjects

The study was approved by the institutional review board of the Beth Israel Deaconess Medical Center. Cases were selected from the Autism Tissue Program and Autism BrainNet brain banking programs and from the neuropathology archives of the Beth Israel Deaconess Medical Center in Boston, MA. We analyzed postmortem brain tissues from 25 ASD and 30 control cases. All tissues were from postmortem cases with informed consent obtained from the next of kin. ASD and control cases with age at death <70 years were reviewed. Exclusion criteria were evidence of a CNS infection, neurodegenerative disease, or other neuropsychiatric disorder where ASD was absent, and additionally for control cases, a known family member with ASD. A history of seizures was documented in 13/25 (52%) of ASD and 8/30 (27%) of control cases. Additional clinical and other case data, including brain weight, are shown in Table 1. One of the control cases, C18, had a mutation in CDKL5 and early infantile epileptic encephalopathy. ASD cases include those with known point mutations in A1, A2, and A3, XYY karyotype in A4, and chromosome 15q duplication in A5.

Histology and Immunohistochemical staining

The brain region sample distribution was similar for ASD and control cases. Samples were processed following standard histologic methods: following formalin fixation and paraffin embedding, tissue blocks were cut into 5 μm-thick sections for all samples, mounted on glass slides, and stained with hematoxylin and eosin and Luxol Fast Blue (H&E+LFB). All

available blocks containing cerebral cortex were also used for Masson's Trichrome staining (collagen). Following automated lymphocyte quantification (see below), blocks from each case (ASD and control) with the highest lymphocyte counts were selected for staining with primary antibodies raised against CD3, CD20, CD4, and CD8 using avidin-biotin immunohistochemistry (IHC). Standard immunohistochemical staining protocols were followed using 5 μm-thick sections taken from the formalin-fixed paraffin embedded tissue blocks. A single antibody per slide was applied to sequential sections from the blocks. The block from each case with the largest median perivascular space identified on H&E was selected for staining with GFAP and CD68. Blocks from selected autism cases with largest median perivascular space were additionally stained with S100b and ALDH1L1. Control staining was performed for all primary antibodies used in the study and did not show background staining.

Automated lymphocyte detection and segmentation procedure

All available H&E+LFB stained slides were reviewed with a standard bright field microscope and photographs were taken using a 60x objective (600x total magnification; TIFF-format; resolution 2448x1920 pixels) using a 5-megapixel CCD camera (Model DP27, Olympus). On every H&E+LFB-stained section from every ASD and control case, while blinded to the diagnosis, we photographed three blood vessels with the most abundant perivascular lymphocytes in each of the following brain compartments: grey matter, white matter, or leptomeninges. Fields containing single vessels (luminal diameter range 15-500μm) involved by the highest density of lymphocytes were selected from ASD and control cases using a 40x objective. This resulted in a collection of images with identical field of view sizes.

All images were then analyzed using a custom-built program in MATLAB (Mathworks Inc, Natick, MA) to perform the following operations: convert the original RGB image to HSV color space. Smooth the hue channel using a Gaussian kernel with σ=80, and then threshold around the largest hue peak between [0.55, 0.8] to create a mask for white matter. Smooth the value channel using a Gaussian kernel with σ=5, and apply an Otsu automatic threshold. To eliminate white matter oligodendroglia from further analysis, apply the inverse of the white matter mask to the smoothed value channel. Next, apply the morphologic opening operation, followed by watershed segmentation. Then, erode with a disc structuring element (4-pixel diameter). Delete regions with areas outside lymphocyte size range as expected for the known image magnification. Delete regions for which $4*\pi*\text{Area}/\text{Perimeter}^2 < 0.5$ (to loosely enforce circularity). Apply the circular Hough Transform algorithm for circle identification (radius range 10-20 pixels, sensitivity 0.99, edge gradient threshold 0.95). Finally, threshold circle regions on the mean of the saturation channel. Return a list of statistics for each circular region of interest (ROI): area, centroid, eccentricity, mean intensity, perimeter.

All circular ROIs were marked on H&E+LFB images, with their mean saturations. All output images were manually reviewed for accuracy, and if cell nuclei were misidentified as lymphocytes or if lymphocyte nuclei were missed, cell counts for the images were manually

corrected. This procedure resulted in identification of 29,549 lymphocytes involving 1,868 vessels across 9 brain regions in the entire study set.

Automated white matter perivascular space segmentation procedure

All available H&E+LFB stained slides were reviewed with a standard bright field microscope with camera, as described above. The ten white matter vessels surrounded by the largest space intervening between the vessel wall and white matter parenchyma were selected from ASD and control cases using a 20x objective and photographed (200x total magnification).

All images were analyzed using a custom-built program in MATLAB to perform the following operations: down sample image by a factor of 4. Color threshold RGB image to find LFB stained regions (based on a composite example LFB image). Morphologic close with 4-pixel radius disk element. Fill holes and apply resulting mask to original RGB image, convert to LAB color space. Apply contrast-limited adaptive histogram equalization to “B” channel using 64 tiles. Convert to gray scale. Subtract smoothed version of image (Gaussian kernel, sigma =16 pixels). Apply an Otsu threshold, and apply a morphologic closing operation.

The resulting ROI was taken as the mask whose edges were defined by the boundary of the LFB staining around the photographed vessel. This ROI served as the basis for area and boundary contour measurements.

Automated trichrome perivascular collagen segmentation procedure

Trichrome stained slides created from all available blocks containing cerebral cortex were reviewed with a standard bright field microscope and camera using a 20x objective, as described above. Six blood vessels in white matter surrounded by the largest amount of blue stained perivascular collagen among all blocks for each ASD and control case were photographed using a 20x objective (200x total magnification).

All images were then analyzed using a custom-built MATLAB program to perform the following operations: down sample image by a factor of 4 and convert to LAB color space. Z-score “a” and “b” channels. Threshold color based on distance in “ab” space from a defined center color (less than 1.75 from (−6,1)). Apply image dilation and morphologic opening to resulting mask, and fill holes. Find boundaries in mask, retain regions enclosed by boundaries that are connected to the most central region by space no more than 2% of the image width (Dijkstra algorithm), in order to eliminate any blue-staining regions not associated with the vessel of interest. Fill holes, and apply an erode mask using a 12-pixel diameter disk element.

This provided a coarse mask for the blue-staining collagen in the images. A second color threshold based on distance to the center in color space was then applied within this coarse mask applied to the LAB image, and the result was used for the final measurement of collagen area. The largest enclosed area inside the coarse mask (i.e. largest hole in the mask) after a dilation by a 12-pixel diameter disk element was taken as the lumen area and used as a normalization for the collagen area.

Immunohistochemistry image acquisition and analysis

Using a 40x objective (400x total magnification), we photographed ten of the white matter blood vessels with the most abundant perivascular GFAP debris signal across all blocks containing cerebral cortex in each case of the ASD and control cases to quantify perivascular GFAP+ debris in white matter. MATLAB software was used to deconvolve the 3,3'-diaminobenzidine color channel, smooth it, threshold it, and measure the total positively stained area after manual masking of surrounding positively stained material in the brain parenchyma.

CD3 stained slides were imaged on a whole-slide scanning system using raster scan following manual focal point selection. The resulting whole-slide images were analyzed using a combination of direct cell density measurement with QuPath histology image analysis software[9] and a custom written program in Python using the ImageJ libraries to process images tile by tile after import with the BioFormats plugin. After color deconvolution to separate the 3,3'-diaminobenzidine-stained regions, images were smoothed and thresholded, followed by morphologic opening, erosion, and watershed segmentation, after which the ImageJ particle analyzer was used to identify stained regions with size greater than 12 μm and circularity in the range 0.4-1.0.

CD4, CD8, and CD20 stained slides were manually reviewed and the ten fields of view (40x objective; 400x total magnification) containing the highest cell counts for ASD and control cases were photographed. Lymphocytes (CD4, CD8, and CD20 stains) were manually counted.

We photographed at 100x total magnification five of the white matter blood vessels with the most abundant perivascular space CD68 signal in each ASD and control case and quantified the number and cytoplasmic area of CD68+ cells. The CD68 images were additionally quantified using MATLAB software to deconvolve the 3,3'-diaminobenzidine color channel, smooth it, threshold it, and measure the total positively stained area.

Statistical Methods

All images were analyzed using custom-designed algorithms implemented in MATLAB (MathWorks, Natick MA) as described above. Cells and tissue structures of interest were segmented on all images and all segmentation results were validated by manual inspection by two pathologists. The segmented regions of interest were the basis for morphologic measurements on each area, including cell counts, areas, perimeters, and jaggedness (squared second derivative of perimeter contour). Statistical inferences for continuous variables were made using Welch's t-tests, ANOVA with Tukey's post-hoc comparison of means, simple linear regression, Kendall's rank-order correlation for non-normally distributed variables, and receiver operating characteristic curves, all implemented in R.

Results

Damage of CSF-brain barrier astrocyte processes in autism spectrum disorder

We observed a unique histologic feature in the perivascular Virchow-Robin cerebrospinal fluid (CSF) spaces of some of the small caliber blood vessels in the brain from some individuals with ASD that was absent from the controls: round and uniformly eosinophilic membranous blebs of varying sizes (see H&E+LFB stained sections in Fig. 1A). These membranous blebs (pale blue in Fig. 1B) were often in proximity to $CD8^+$ lymphocytes. Immunohistochemistry for astrocyte marker glial fibrillary acidic protein (GFAP) revealed strong positive staining of the membranous blebs with some blebs contiguous with long narrow astrocytic processes (Fig. 1A). The membranous blebs also stained positive for two additional astrocyte markers, S100B and ALDH1L1, confirming their astrocyte origins. In photomicrographs of white matter blood vessels visually chosen for the most abundant $GFAP^+$ material in each ASD and control case, the area occupied by the perivascular astrocyte blebs (defined as $GFAP^+$ area within the space delimited by the vascular endothelium and white matter edge/glia limitans) was markedly increased in ASD relative to controls (Fig. 1C). In order to rule out an artifact due to postmortem tissue disintegration, cases in which the thin $GFAP^+$ astrocyte processes of the white and grey matter had degraded (fine fibrillary structures lost) were excluded from the analysis. Using the same sampling strategy on sections stained for the macrophage marker CD68, we found an increase in the area of cytoplasmic staining but no increase in total number of $CD68^+$ macrophages in ASD compared to controls in these white matter perivascular spaces (not shown). Reactive microglia were also observed in ASD, but not quantified.

$CD8^+$ cytotoxic T-lymphocytes are increased in autism spectrum disorder

Microscopic visual inspection of H&E+LFB-stained brain sections revealed rare but prominent perivascular lymphocytic cuffs scattered in a semi-random pattern across the brain tissue blocks that were more numerous and prominent in ASD than control brains. This clinical assessment was confirmed using segmentation algorithms with manually tuned parameters (lymphocytes defined by shape and color on H&E). The number of lymphocytes in the most populated perivascular cuffs, visually identified and photographed from each ASD and control case, were increased in ASD compared to controls in grey matter, white matter, and leptomeninges (Fig. 2-3), in the gray and white matter of both male and female subjects (Fig. 3A), across all studied age groups (Fig. 3B), and in most brain regions (Fig. 3C). Amongst the most involved brain parenchymal blood vessels identified in both ASD and control for each case, the lymphocyte count per vessel was 15.0 ± 0.6 in ASD and 5.8 ± 0.4 in controls (mean ± s.e.m.). This difference of means yields $p < 0.01$ by Welch's t-test (statistical significance was also found with a linear mixed-effects model fit). The number of perivascular lymphocytes did not correlate with the history of seizures (Figs. 3D and 3E). When measured across whole slide scanned images containing large regions of cortex and white matter, $CD3^+$ T-lymphocyte densities were increased in ASD relative to control (Fig. 4A-C, 4B inset). Lymphocyte counts were increased in 64% of the autism cases (Fig. 2B), including in two cases with known genetic defects (PTEN and XYY), when using the top 16 blood vessels with the highest lymphocyte counts in each ASD and control case and a median count of 23 lymphocytes that exceeded the control threshold (parameters chosen to

yield ≥ 95% specificity; area under ROC curve = 0.785). Immunohistochemistry revealed that the immune cells are predominantly $CD3^+$ and $CD8^+$ T lymphocytes (Figs. 4B and 4C), along with a smaller population of $CD4^+$ T cells and fewer small clusters of $CD20^+$ B cells. A subset of lymphocytes contained granzyme B^+ cytoplasmic puncta, a T-lymphocyte and NK cell proteolytic effector molecule (Fig. 4A).

The quantities of lymphocytes and astrocyte debris correlate across autism spectrum disorder cases

Importantly, comparison at the case level revealed that the quantity of perivascular $GFAP^+$ debris (median of the 10 most involved vessels; includes the membranous blebs) correlates to the number of lymphocytes (median of the 16 vessels most involved by lymphocyte cuffs) across ASD cases (Fig. 2C).

Perivascular space is increased and has a more jagged contour in autism spectrum disorder

Based on the perivascular distribution of lymphocytes and cell debris and our histologic observation of foci with enlarged perivascular spaces and prominent adventitial collagen in the ASD cases, we performed quantitative measures of these features where most prominent (hereafter referred to as top vessels) in ASD and control cases. Perivascular space, like lymphocyte numbers, was increased around vessels in ASD relative to control when comparing the top 10 vessels (Figs. 5A and 5B), including in the genetic form PTEN+/− (case A2). We also observed a jagged contour to the edge of the perivascular white matter surrounding these top vessels that was increased in ASD relative to control (quantified using a squared second derivative of the contour, designated jaggedness, Fig. 5C), consistent with a segmental cell-mediated damage of perivascular astrocytes. Increased jaggedness was also observed selectively in the two genetic cases of ASD with increased lymphocytes [XYY (case A4) and PTEN+/− (case A2)]. Control and ASD cases are robustly separated in a scatter plot of median perivascular lymphocyte count and median jaggedness index of the top vessels (Fig. 5D), suggesting the combined use of these two parameters better separates ASD from control.

Perivascular fibrosis is increased in autism spectrum disorder

The quantity of perivascular collagen was evaluated by staining with trichrome and measured as the area of blue-stained collagen normalized to vessel lumen area for the six vessels with the most prominent collagen in ASD and control cases (see examples, Fig. 6A). Adventitial perivascular collagen was increased at these top vessels from ASD relative to control (see Fig. 6B), including in ASD with PTEN+/− megalencephaly (case A2).

Other CSF-brain interfaces are also damaged in autism spectrum disorder

Patches of decreased neuronal gene expression have been reported in upper cortical layers of ASD postmortem brains[11], so we examined the upper cortical layers in these ASD brains for evidence of pathology. The neuropil (neuronal processes) of cortical layer I was depleted in a patchy distribution associated with increased $GFAP^+$ staining of subpial astroglia in the ASD cases (not shown). Overlying the pial surface, we observed focal increases of

leptomeningeal perivascular lymphocytes and focal collections of GFAP+ membranous blebs in the subarachnoid space similar to those found in the white matter perivascular spaces in ASD cases (Fig. 7A), suggesting a possible cause of the focal neuropil loss. We quantified the subpial neuropil density from the pial surface through cortical layer I (normalized to neuropil density in deeper cortical layer IV) at the most severely affected regions in ASD and control cases. Neuropil density was reduced in ASD relative to controls in patches running 60-360 μm below the pial surface (Fig. 7B), a location known to contain cortical pyramidal neuron apical dendrites, specialized GABAergic neurons, and various axonal afferent fibers and synapses.

Consistent with an effect of this inflammatory process on additional CSF-brain barriers (ventricle and pia) in ASD, we observed the following additional pathological lesions: 1) focal ependymal cell loss with astroglial scars protruding into the ventricular space lumen (granular ependymitis) and buried ependymal canals (Fig. 7C); 2) focal subpial mineral deposition (not shown); and 3) focal tufts of subpial astrogliosis (not shown). Only two ASD cases contained rare microglial nodules targeting neurons (eosinophilic) in grey matter (not shown).

Discussion

We report rare scattered, but prominent, perivascular lymphocytic infiltrates and associated astrocyte blebs within the Virchow-Robin and subarachnoid CSF spaces in a large proportion of ASD cases across a wide-range of ages (5-68 years). The lymphocyte cuffs contain cytotoxic effector molecule granzyme B and an admixture of cell types including $CD8^+$ and $CD4^+$ T cells, rare $CD20^+$ B cells, and $CD68^+$ macrophages. In some foci, $CD8^+$ and $CD4^+$ T-lymphocytes extend individually into the white and gray matter parenchyma (not shown). The larger lymphocytic cuffs sometimes contain $CD20^+$ B-cells, presumably representing transient immature tertiary lymphoid organs as reported in multiple sclerosis[10], which were often separate from the sites of astrocyte debris with associated $CD8^+$ cytotoxic T-lymphocytes. The increased collagen deposition and expanded perivascular spaces with jagged contours in ASD suggest a destructive effect of the elevated cytotoxic T-lymphocytes. The numbers of perivascular lymphocytes and the amount of $GFAP^+$ debris correlated across ASD cases (Fig. 2C), a finding that suggests cytotoxic T-lymphocytes may generate the astrocyte membranous blebs. Membranous blebs (also called apoptotic bodies) are generated from cells targeted by cytotoxic agents such as granzyme B or TNFα released from T-lymphocytes[11].

Astrocyte-derived membranous blebs have not been observed in other CNS disorders and we suggest they may be generated by a targeted attack of astrocyte processes by cytotoxic T-lymphocytes specifically at the glia limitans surrounding blood vessels and other CFS-brain boundaries. Consistent with our findings of increased $GFAP^+$ astrocyte debris in perivascular Virchow-Robin space CSF in ASD, GFAP is elevated in CSF and serum in a large proportion of individuals with ASD[12]. The strong separation of ASD from control cases on a lymphocyte count vs. jaggedness index scatter plot (Fig. 5D) and the correlation of lymphocyte count with astrocyte debris on a scatter plots of ASD cases (Fig. 2C) suggest these histologic features could be causally connected biomarkers of the ASD pathogenic

process. Our findings suggest future diagnostic evaluations and research of ASD postmortem brains should examine the following: (1) perivascular $CD8^+$ T-lymphocyte infiltrates, (2) CSF-glia limitans barrier damage (including increased perivascular space and collagen deposition), and (3) $GFAP^+$ astrocyte membranous blebs in CSF space compartments.

We suggest the invading $CD8^+$ lymphocytes in ASD may have T cell receptors that selectively target epitope(s) presented by MHC-expressing astrocytes localized at the glia limitans where $CD8^+$ T-cell cytotoxic effectors such as granzyme B may be locally released to generate these $GFAP^+$ astrocyte membranous blebs in ASD. An MRI study has revealed dilated Virchow-Robin spaces in the centrum semiovale white matter in 7 of 16 subjects with ASD[13]; a possible correlate to the dilated perivascular spaces we identified in white matter. Astrocyte debris released into the Virchow-Robin CSF spaces and leptomeningeal fibrosis (collagen deposition) could contribute to other brain pathologic processes such the obstruct of CSF absorption consistent with the evidence of increased extra-axial cerebrospinal fluid in high-risk infants that develop ASD[14]. The astrocyte-targeted damage could have direct or indirect (cytokine-mediated) immune effects on the ability of astrocytes to provide metabolic support to axons causing action potential transmission failures[15] as one explanation for the long-range functional connectivity deficits documented in ASD[16].

This $CD8^+$ T-lymphocyte-rich immune neuropathology of ASD and that of other $CD8^+$ T-lymphocyte-rich immune disorders of the CNS are distinct in two ways: 1) the brain tissue compartments infiltrated by T-lymphocytes, and 2) the cell types attacked by the T-lymphocytes. In multiple sclerosis, $CD8^+$ T-lymphocytes are found in perivascular cuffs, but also extend more deeply into the white matter where they attack oligodendrocytes to demyelinate axons and produce myelin debris[17,18]. In Rasmussen's encephalitis, $CD8^+$ T lymphocytes are found in perivascular cuffs, but also infiltrate cortical grey matter where they attack and destroy pyramidal neurons[19]. ASD has $CD8^+$ T-lymphocytes in brain perivascular cuffs, but has limited or no evidence of white matter demyelination, myelin debris, or cortical neuron destruction, and instead associates with $GFAP^+$ membranous bleb debris co-localized with and sometimes in continuity with the glia limitans perivascular astrocytes in ASD.

Analogous rare microscopic foci of activated immune cell attack occurs in polymyositis, an inflammatory myopathy of skeletal muscle that generates organ dysfunctions well beyond these microscopic foci. In addition to the minute foci of cytotoxic $CD8^+$ T-lymphocyte attack that generate myocyte necrosis there is more widespread transcriptional changes including for example increased major histocompatibility complex (MHC) class antigen expression and clinical evidence of muscle weakness[20].

In Type 1 Diabetes (T1D), a $CD8^+$ T-lymphocyte autoimmune disorder of early childhood, specific MHC variants bind and present self-antigens to cytotoxic $CD8^+$ T cells to promote pancreatic islet cell destruction[21,22]. Like T1D, specific MHC alleles have been found in ASD[23]. Our data suggest these ASD-associated MHC alleles might play a role in presenting antigens to the $CD8^+$ T-lymphocyte infiltrates found in the ASD brain. T1D is initiated and possibly sustained by viral infections[24]. While histologic evidence of typical CNS viral

infections and immunohistochemical staining for HSV1, HSV2, VZV, CMV, and JC virus were negative (not shown), a potential role of infection in initiating or sustaining this T-lymphocyte immune response in ASD remains an important consideration.

Autism cases A2 (PTEN megalencephaly) and A4 (XYY) were affected by the same T-lymphocyte and astroglial neuropathology as the idiopathic ASD cases. Importantly, PTEN heterozygosity is associated with lymphoid hyperplasia and an increased risk of autoimmune disease in human and mouse[25,26]. Similarly, XYY is a genetic defect reported in ASD cohorts[27] and genes on the Y chromosome have been connected to an increased risk of immunologic disease[28]. By contrast, ASD case A1 (mutations in ARID1B, CACNA1C, and SLC6A8), ASD case A3 (mutation in SETD2), ASD case A5 (dup15q), and another ~30% of the ASD cases that are genetically-undefined lacked features of the T-lymphocyte and astroglial neuropathology suggesting behavioral deficits in these genetic subsets of ASD might instead arise from direct effects of the genetic or epigenetic changes on the neuronal circuits controlling behaviors impaired in ASD[29-35].

$CD8^+$ T-lymphocyte infiltrates and cytotoxic astrocyte membranous blebs represent a new cellular process not previously reported in studies of ASD neuropathology[36-40]. Future research should test if the maternal-fetal[41-50] or autoimmune[51-54] antibodies found in the serum in some cases of ASD co-occur with the $CD8^+$ T-lymphocyte immune cell infiltrates and astrocyte membranous blebs or represent a separate autoimmune subtype of ASD. Autoantibodies, targeting multiple distinct pancreatic islet cell epitopes, co-occur with $CD8^+$ cytotoxic T-lymphocyte attack of islet cells in T1D[22]. Our study provides signature features of this T-lymphocyte immune subtype of ASD in postmortem cases and identifies astrocyte debris as a potential source of CSF or serum biomarkers for clinical diagnosis and monitoring of the pathology in living patients. Finally, with biomarkers that define the T-lymphocyte immune subtype of ASD, the efficacy of T-lymphocyte-targeted immunotherapies on biomarker levels and behavioral symptoms could be tested.

Acknowledgements

We thank Autism BrainNet, a resource of the Simons Foundation Autism Research Initiative, now including also the Autism Speaks, Autism Tissue Program (ATP) collection. We are grateful and indebted to the families who donated tissue for research purposes to Autism BrainNet and the ATP. We also thank Jane Pickett, PhD, Cynthia M. Schumann, PhD, Carol A. Tamminga, MD, Patrick R. Hof, MD, and Carolyn K. Hare, MS, for their help in acquiring the brain samples and clinical details. We thank Patrick R. Hof, MD and Ken Swanson, PhD for reading and editing the manuscript. We thank the Boston Children's Hospital IDDRC (U54 HD090255, P30 HD18655) and other funding to M.P.A. from The National Institute of Mental Health (R01 MH114858, R01 MH112714), The National Institute of Neurological Disorders and Stroke (R01 NS08916), The Nancy Lurie Marks Family Foundation, The Landreth Foundation, Autism Speaks/National Alliance for Autism Research, and the Simons Foundation/Autism BrainNet (FA#345171).

REFERENCES

1. Vargas DL, Nascimbene C, Krishnan C, Zimmerman AW, Pardo CA. Neuroglial activation and neuroinflammation in the brain of patients with autism. Annals of neurology 2005;57:67–81. [PubMed: 15546155]
2. Laurence JA, Fatemi SH. Glial fibrillary acidic protein is elevated in superior frontal, parietal and cerebellar cortices of autistic subjects. Cerebellum 2005;4:206–10. [PubMed: 16147953]

3. Morgan JT, Chana G, Pardo CA, et al. Microglial activation and increased microglial density observed in the dorsolateral prefrontal cortex in autism. Biological psychiatry 2010;68:368–76. [PubMed: 20674603]
4. Suzuki K, Sugihara G, Ouchi Y, et al. Microglial activation in young adults with autism spectrum disorder. JAMA psychiatry 2013;70:49–58. [PubMed: 23404112]
5. Morgan JT, Barger N, Amaral DG, Schumann CM. Stereological study of amygdala glial populations in adolescents and adults with autism spectrum disorder. PloS one 2014;9:e110356. [PubMed: 25330013]
6. Garbett K, Ebert PJ, Mitchell A, et al. Immune transcriptome alterations in the temporal cortex of subjects with autism. Neurobiology of disease 2008;30:303–11. [PubMed: 18378158]
7. Voineagu I, Wang X, Johnston P, et al. Transcriptomic analysis of autistic brain reveals convergent molecular pathology. Nature 2011;474:380–4. [PubMed: 21614001]
8. Gupta S, Ellis SE, Ashar FN, et al. Transcriptome analysis reveals dysregulation of innate immune response genes and neuronal activity-dependent genes in autism. Nature communications 2014;5:5748.
9. Bankhead Peter, et al. “QuPath: Open Source Software for Digital Pathology Image Analysis.” Scientific Reports 2017, vol. 7, no. 1, p. 16878 [PubMed: 29203879]
10. Mitsdoerffer M, Peters A. Tertiary Lymphoid Organs in Central Nervous System Autoimmunity. Frontiers in Immunology. 2016; 7: 451 [PubMed: 27826298]
11. Poon IK, Lucas CD, Rossi AG, Ravichandran KS. Apoptotic cell clearance: basic biology and therapeutic potential. Nature reviews Immunology 2014;14:166–80.
12. Esnafoglu E, Ayyildiz SN, Cirrik S, et al. Evaluation of serum Neuron-specific enolase, S100B, myelin basic protein and glial fibrilliary acidic protein as brain specific proteins in children with autism spectrum disorder. International journal of developmental neuroscience : the official journal of the International Society for Developmental Neuroscience 2017;61:86–91. [PubMed: 28711670]
13. Taber KH, Shaw JB, Loveland KA, Pearson DA, Lane DM, Hayman LA. Accentuated Virchow-Robin spaces in the centrum semiovale in children with autistic disorder. Journal of computer assisted tomography 2004;28:263–8. [PubMed: 15091132]
14. Shen MD, Kim SH, McKinstry RC, et al. Increased Extra-axial Cerebrospinal Fluid in High-Risk Infants Who Later Develop Autism. Biological psychiatry 2017;82:186–93. [PubMed: 28392081]
15. Wender R, Brown AM, Fern R, Swanson RA, Farrell K, Ransom BR. Astrocytic glycogen influences axon function and survival during glucose deprivation in central white matter. The Journal of neuroscience : the official journal of the Society for Neuroscience 2000;20:6804–10. [PubMed: 10995824]
16. Rane P, Cochran D, Hodge SM, Haselgrove C, Kennedy DN, Frazier JA. Connectivity in Autism: A Review of MRI Connectivity Studies. Harvard review of psychiatry 2015;23:223–44. [PubMed: 26146755]
17. Hauser SL, Bhan AK, Gilles F, Kemp M, Kerr C, Weiner HL. Immunohistochemical analysis of the cellular infiltrate in multiple sclerosis lesions. Annals of neurology 1986;19:578–87. [PubMed: 3524414]
18. Babbe H, Roers A, Waisman A, et al. Clonal expansions of CD8(+) T cells dominate the T cell infiltrate in active multiple sclerosis lesions as shown by micromanipulation and single cell polymerase chain reaction. The Journal of experimental medicine 2000;192:393–404. [PubMed: 10934227]
19. Bien CG, Bauer J, Deckwerth TL, et al. Destruction of neurons by cytotoxic T cells: a new pathogenic mechanism in Rasmussen's encephalitis. Annals of neurology 2002;51:311–8. [PubMed: 11891826]
20. Dorph C, Englund P, Nennesmo I, et al. Signs of inflammation in both symptomatic and asymptomatic muscles from patients with polymyositis and dermatomyositis. Ann Rheum Dis. 2006 12;65(12):1565–71. [PubMed: 16831829]
21. Jerram ST, Leslie RD. The Genetic Architecture of Type 1 Diabetes. Genes 2017;8.
22. Redondo MJ, Steck AK, Pugliese A. Genetics of type 1 diabetes. Pediatric diabetes 2018;19:346–53. [PubMed: 29094512]

23. Torres AR, Sweeten TL, Johnson RC, et al. Common Genetic Variants Found in HLA and KIR Immune Genes in Autism Spectrum Disorder. Frontiers in neuroscience 2016;10:463. [PubMed: 27812316]
24. Allen DW, Kim KW, Rawlinson WD, Craig ME. Maternal virus infections in pregnancy and type 1 diabetes in their offspring: Systematic review and meta-analysis of observational studies. Reviews in medical virology 2018;28:e1974. [PubMed: 29569297]
25. Di Cristofano A, Kotsi P, Peng YF, Cordon-Cardo C, Elkon KB, Pandolfi PP. Impaired Fas response and autoimmunity in Pten+/− mice. Science 1999;285:2122–5. [PubMed: 10497129]
26. Chen HH, Handel N, Ngeow J, et al. Immune dysregulation in patients with PTEN hamartoma tumor syndrome: Analysis of FOXP3 regulatory T cells. The Journal of allergy and clinical immunology 2017;139:607–20 e15. [PubMed: 27477328]
27. Tartaglia NR, Wilson R, Miller JS, et al. Autism Spectrum Disorder in Males with Sex Chromosome Aneuploidy: XXY/Klinefelter Syndrome, XYY, and XXYY. Journal of developmental and behavioral pediatrics : JDBP 2017;38:197–207. [PubMed: 28333849]
28. Teuscher C, Noubade R, Spach K, et al. Evidence that the Y chromosome influences autoimmune disease in male and female mice. Proceedings of the National Academy of Sciences of the United States of America 2006;103:8024–9. [PubMed: 16702550]
29. Krishnan V, Stoppel DC, Nong Y, et al. Autism gene Ube3a and seizures impair sociability by repressing VTA Cbln1. Nature 2017;543:507–12. [PubMed: 28297715]
30. Smith SE, Zhou YD, Zhang G, Jin Z, Stoppel DC, Anderson MP. Increased gene dosage of Ube3a results in autism traits and decreased glutamate synaptic transmission in mice. Science translational medicine 2011;3:103ra97.
31. Peca J, Feliciano C, Ting JT, et al. Shank3 mutant mice display autistic-like behaviours and striatal dysfunction. Nature 2011;472:437–42. [PubMed: 21423165]
32. Penagarikano O, Abrahams BS, Herman EI, et al. Absence of CNTNAP2 leads to epilepsy, neuronal migration abnormalities, and core autism-related deficits. Cell 2011;147:235–46. [PubMed: 21962519]
33. Clement JP, Aceti M, Creson TK, et al. Pathogenic SYNGAP1 mutations impair cognitive development by disrupting maturation of dendritic spine synapses. Cell 2012;151:709–23. [PubMed: 23141534]
34. Han S, Tai C, Westenbroek RE, et al. Autistic-like behaviour in Scn1a+/− mice and rescue by enhanced GABA-mediated neurotransmission. Nature 2012;489:385–90. [PubMed: 22914087]
35. Won H, Lee HR, Gee HY, et al. Autistic-like social behaviour in Shank2-mutant mice improved by restoring NMDA receptor function. Nature 2012;486:261–5. [PubMed: 22699620]
36. Anderson MP. Autism Spectrum Disorders In: Adle-Biassette BH, Jeffrey Golden, ed. Developmental Neuropathology: Wiley-Blackwell; 2018:477–95.
37. Pardo CA, Vargas DL, Zimmerman AW. Immunity, neuroglia and neuroinflammation in autism. International review of psychiatry 2005;17:485–95. [PubMed: 16401547]
38. Bauman ML, Kemper TL. Neuroanatomic observations of the brain in autism: a review and future directions. International journal of developmental neuroscience : the official journal of the International Society for Developmental Neuroscience 2005;23:183–7. [PubMed: 15749244]
39. Blatt GJ. The neuropathology of autism. Scientifica 2012;2012:703675. [PubMed: 24278731]
40. Hutsler JJ, Casanova MF. Review: Cortical construction in autism spectrum disorder: columns, connectivity and the subplate. Neuropathology and applied neurobiology 2016;42:115–34. [PubMed: 25630827]
41. Warren RP, Cole P, Odell JD, et al. Detection of maternal antibodies in infantile autism. Journal of the American Academy of Child and Adolescent Psychiatry 1990;29:873–7. [PubMed: 2273013]
42. Dalton P, Deacon R, Blamire A, et al. Maternal neuronal antibodies associated with autism and a language disorder. Annals of neurology 2003;53:533–7. [PubMed: 12666123]
43. Braunschweig D, Ashwood P, Krakowiak P, et al. Autism: maternally derived antibodies specific for fetal brain proteins. Neurotoxicology 2008;29:226–31. [PubMed: 18078998]
44. Zimmerman AW, Connors SL, Matteson KJ, et al. Maternal antibrain antibodies in autism. Brain, behavior, and immunity 2007;21:351–7.

45. Singer HS, Morris CM, Gause CD, Gillin PK, Crawford S, Zimmerman AW. Antibodies against fetal brain in sera of mothers with autistic children. Journal of neuroimmunology 2008;194:165–72. [PubMed: 18093664]

46. Croen LA, Braunschweig D, Haapanen L, et al. Maternal mid-pregnancy autoantibodies to fetal brain protein: the early markers for autism study. Biological psychiatry 2008;64:583–8. [PubMed: 18571628]

47. Braunschweig D, Duncanson P, Boyce R, et al. Behavioral correlates of maternal antibody status among children with autism. Journal of autism and developmental disorders 2012;42:1435–45. [PubMed: 22012245]

48. Rossi CC, Fuentes J, Van de Water J, Amaral DG. Brief Report: Antibodies Reacting to Brain Tissue in Basque Spanish Children with Autism Spectrum Disorder and Their Mothers. Journal of autism and developmental disorders 2013.

49. Brimberg L, Sadiq A, Gregersen PK, Diamond B. Brain-reactive IgG correlates with autoimmunity in mothers of a child with an autism spectrum disorder. Molecular psychiatry 2013;18:1171–7. [PubMed: 23958959]

50. Jones KL, Van de Water J. Maternal autoantibody related autism: mechanisms and pathways. Molecular psychiatry 2018.

51. Singer HS, Morris CM, Williams PN, Yoon DY, Hong JJ, Zimmerman AW. Antibrain antibodies in children with autism and their unaffected siblings. Journal of neuroimmunology 2006;178:149–55. [PubMed: 16842863]

52. Goines P, Haapanen L, Boyce R, et al. Autoantibodies to cerebellum in children with autism associate with behavior. Brain, behavior, and immunity 2011;25:514–23.

53. Wills S, Rossi CC, Bennett J, et al. Further characterization of autoantibodies to GABAergic neurons in the central nervous system produced by a subset of children with autism. Molecular autism 2011;2:5. [PubMed: 21521495]

54. Quadros EV, Sequeira JM, Brown WT, et al. Folate receptor autoantibodies are prevalent in children diagnosed with autism spectrum disorder, their normal siblings and parents. Autism research : official journal of the International Society for Autism Research 2018;11:707–12. [PubMed: 29394471]

55. D'Gama AM, Pochareddy S, Li M, et al. Targeted DNA Sequencing from Autism Spectrum Disorder Brains Implicates Multiple Genetic Mechanisms. Neuron 2015;88:910–7. [PubMed: 26637798]

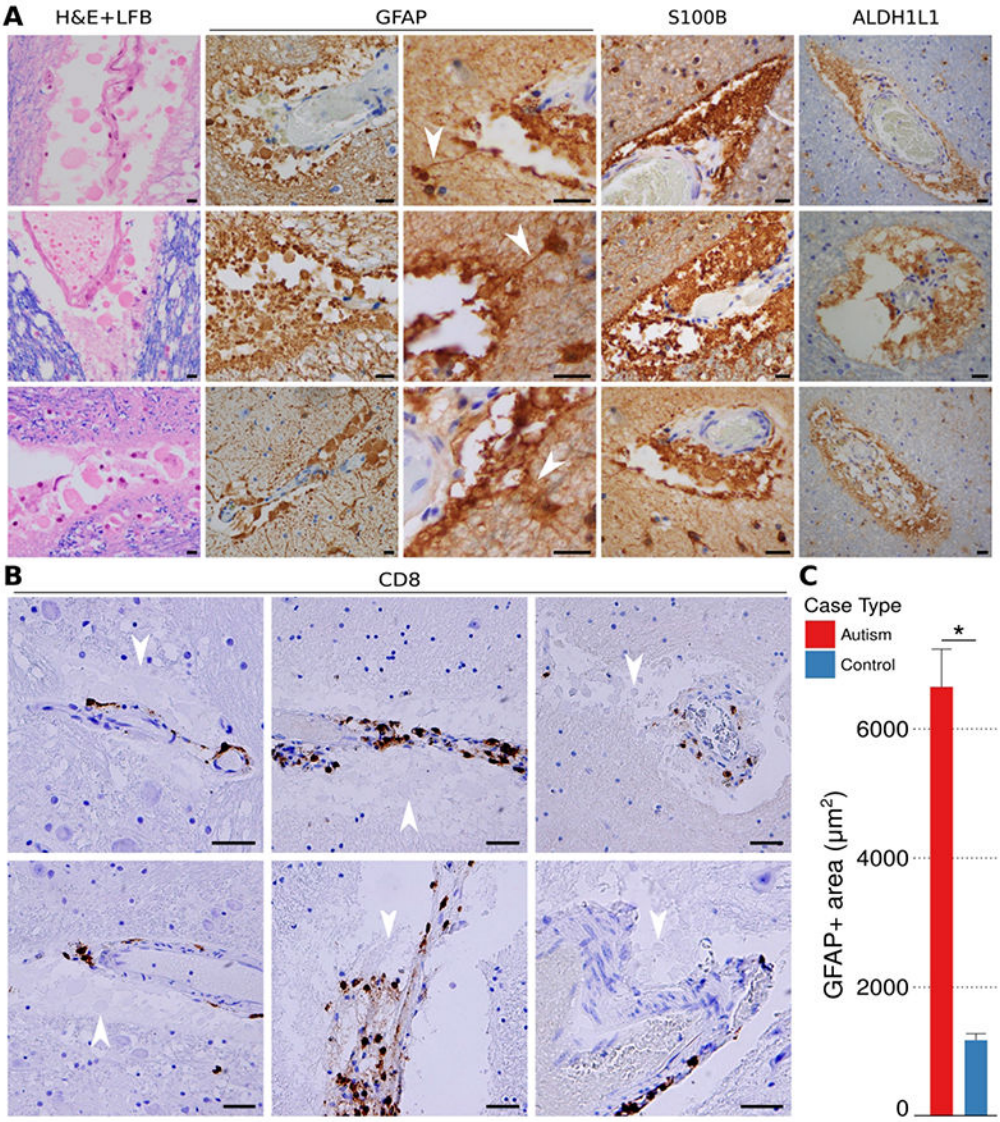

Figure 1. Perivascular membranous blebs stain with multiple astrocyte markers and co-localize with CD8+ T-cells in ASD brains.

Round and uniformly eosinophilic membranous blebs of varying sizes were identified in the perivascular Virchow-Robin spaces of autism brains (white matter examples, A; all scale bars, 40 μm). The membranous blebs are eosinophilic on H&E+LFB (A, column 1). GFAP, S100, and ALDHL1 immunohistochemical staining (A, columns 2-4) establishes the blebs as derived from astrocytes. Photomicrographs taken from gray and white matter samples from ASD brain cases double stained by immunohistochemistry for CD8 and hematoxylin reveal the cytotoxic $CD8^+$ T-cells (brown) in close proximity to membranous blebs (B; pale blue, white arrowheads; all scale bars, 40 μm). Perivascular GFAP+ material was increased in autism compared to controls (C, $N_{vessels}$autism] = 209, $N_{vessels}$[control] = 120). Bar heights represent means and whiskers represent s.e.m. * = $p < 0.05$, Welch's t-test.

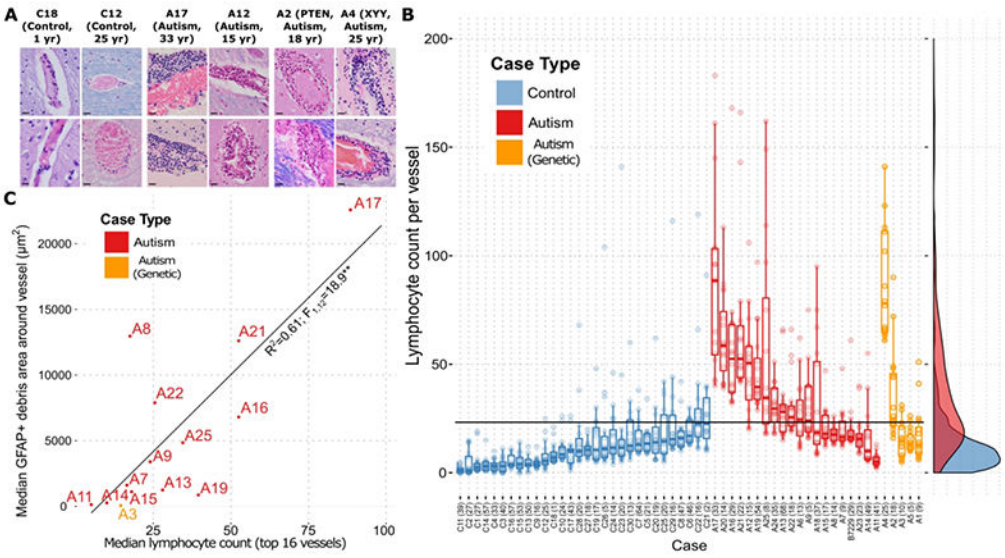

Figure 2. Lymphocytes are increased in cuffs around a subset of vessels, and their numbers correlate to the quantity of perivascular GFAP+ membranous blebs across ASD cases.

Representative images of blood vessels in the brain parenchyma of two control patients and four patients carrying an autism diagnosis show increased abundance of aggregated perivascular lymphocytes in the autism cases (A; all scale bars represent 40 μm). Perivascular lymphocyte counts for each of the top vessels (up to 16) in every case identified by comprehensive visual inspection of the slides show an increase in ASD compared to control cases (B). Dots represent lymphocyte counts for each vessel. Overlaid box-and-whisker plots represent the medians, upper and lower quartiles, and upper/lower quartiles ± 1.5*(interquartile range). Smoothed density plots for all cases are shown on right margin. X-axis labels are case names, with years of age in parentheses. The horizontal black “cutoff” line represents the lymphocyte count of 23 that gives the highest sensitivity for autism vs. control while preserving 95% specificity. The aggregate differences between autism and control counts are statistically significant ($p < 0.0005$; ANOVA with Tukey’s post-hoc comparison of means), as are the difference between genetic autism and control ($p < 0.0005$), but not the difference between autism and genetic autism ($p = 0.098$) ($N_{vessels}$[autism] = 336, $N_{vessels}$[control] = 272, $N_{vessels}$[genetic autism] = 64). A plot of perivascular GFAP+ debris against perivascular lymphocyte counts (top up to 16 vessels) for each case shows the correlation between astrocyte-derived debris and lymphocyte numbers (C). ** = $p < 0.001$ for linear regression; the rank-order correlation has a Kendall’s tau of 0.51 ($p=0.01$).

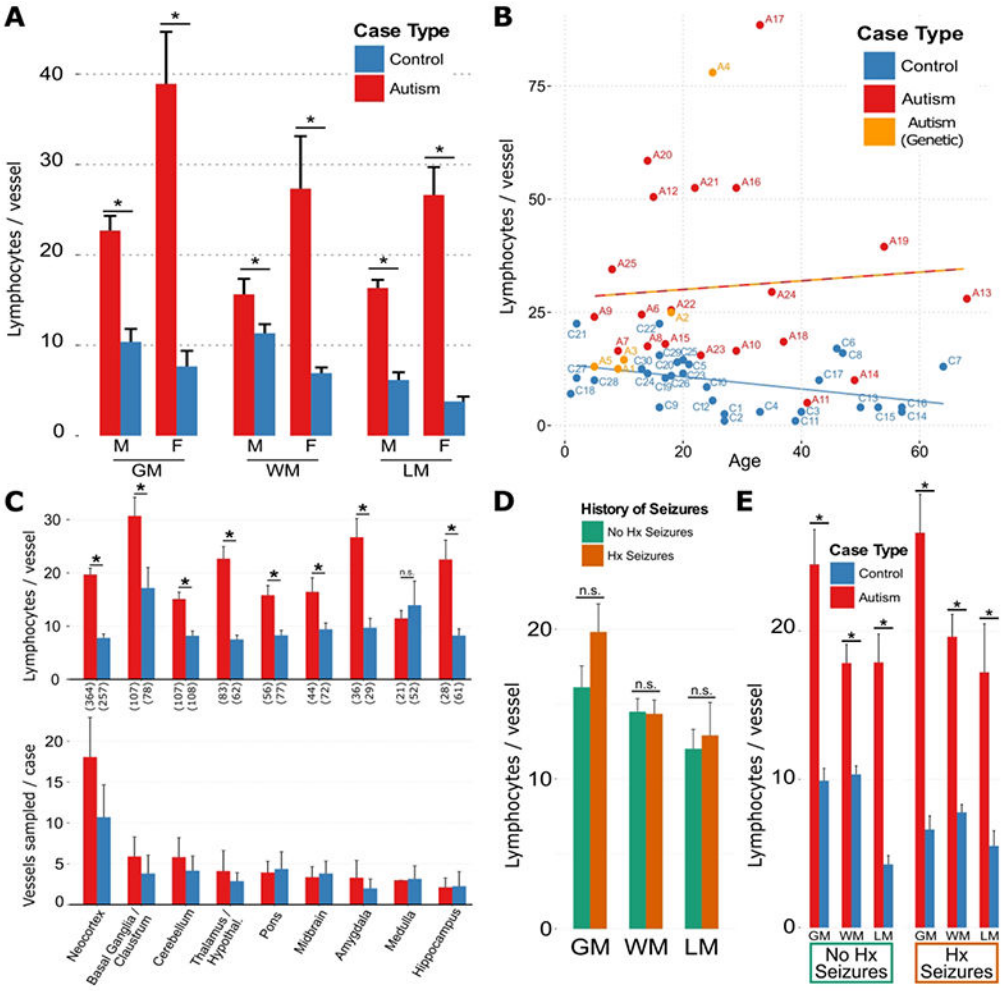

Figure 3. Perivascular cuff lymphocytes are increased across brain regions, compartments and ages in ASD.

(A) Perivascular lymphocyte counts in grey matter (GM), white matter (WM), and leptomeningeal (LM) compartments, separated by sex; * = p < 1e-15, multiple linear regression (MLR) for control vs. autism, controlling for sex and compartment. (B) Median perivascular lymphocyte counts among the top 16 vessels for each case, plotted by age for autism, control and genetic autism cases show that an increase in autism relative to control. The two lines in (B) representing a linear regression of lymphocyte count vs. age for control (blue) and autism (red-orange; includes genetic autism) and show a separation of the groups with diverging upward trend for autism and downward trend for controls of lymphocyte numbers with increasing age. (C, top) Perivascular lymphocyte counts across brain regions were higher in all regions except for medulla in autism (including genetic autism) cases compared with control cases; * = p<0.05, Welch's t-test; n.s. = not significant. Number of sampled vessels across all cases are in parentheses along the abscissa. (C, bottom) Sampling of vessels in this study was similar across brain regions, for autism compared with control cases. The mean±s.e.m. total number of vessels sampled per case was 42.6±10.9 for autism cases and 25.8±15.1 for control cases. Bar heights and whiskers represent mean±s.e.m. number of vessels sampled per case from each brain region for autism and control cases. (D,

E) The effect of history of seizure on perivascular lymphocyte count in autism and control cases was not sufficient to explain the observed difference in lymphocyte counts; * = $p < 0.05$, Welch's t-test. n.s. = not significant. In a multilinear regression (MLR) prediction of number of lymphocytes, it was found that case type (autism or control) was a significant predictor ($\beta = 14.5$, $p < 1e\text{-}15$), but history of seizures ($\beta = 2.3$, $p = 0.07$), and the interaction between autism and seizure history ($\beta = 0.7$, $p = 0.76$) were not. Bar heights in all panels represent means, whiskers represent standard errors of the mean (s.e.m.). For all panels, $N_{vessels}$[autism] = 846, $N_{vessels}$[control] = 796.

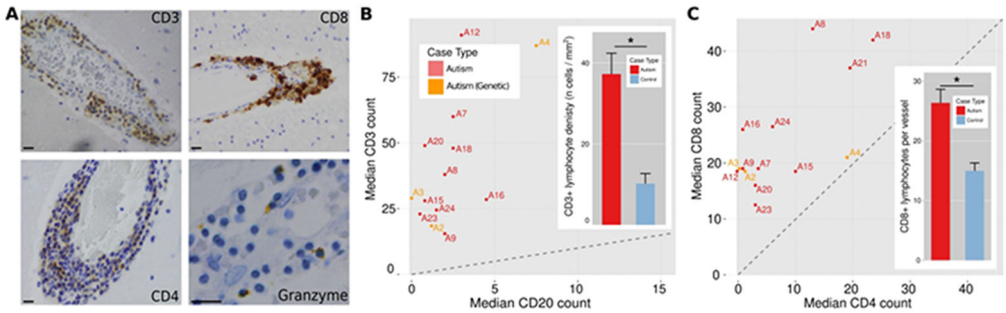

Figure 4. CD8$^+$ cytotoxic T-lymphocytes predominate in the focal perivascular cuffs in ASD brains.

Representative photomicrographs of CD3, CD8, CD4, and granzyme B immunohistochemical stained perivascular lymphocytic cuffs in autism cases (A). Comparison of the median per-vessel CD3$^+$ and CD20$^+$ lymphocyte counts for the autism cases (B) and a comparison of mean ± s.e.m. density of total CD3$^+$ count across whole slides for autism and control cases (B, inset; N_{cases}[autism] = 18, N_{casas} [control] = 21; * = $p < 0.001$). ASD cases fall above the diagonal (dotted line), indicating CD3$^+$ T-cell predominance. Comparison of the median per-vessel CD8$^+$ and CD4$^+$ lymphocyte counts for the autism cases (C) and a comparison of mean ± s.e.m. perivascular CD8$^+$ lymphocyte counts for the autism and control cases (C, inset; $N_{vessels}$[autism] = 66, $N_{vessels}$[control] = 62; * = $p < 0.001$). ASD cases fall above the diagonal, indicating CD8+ cytotoxic T-cell predominance.

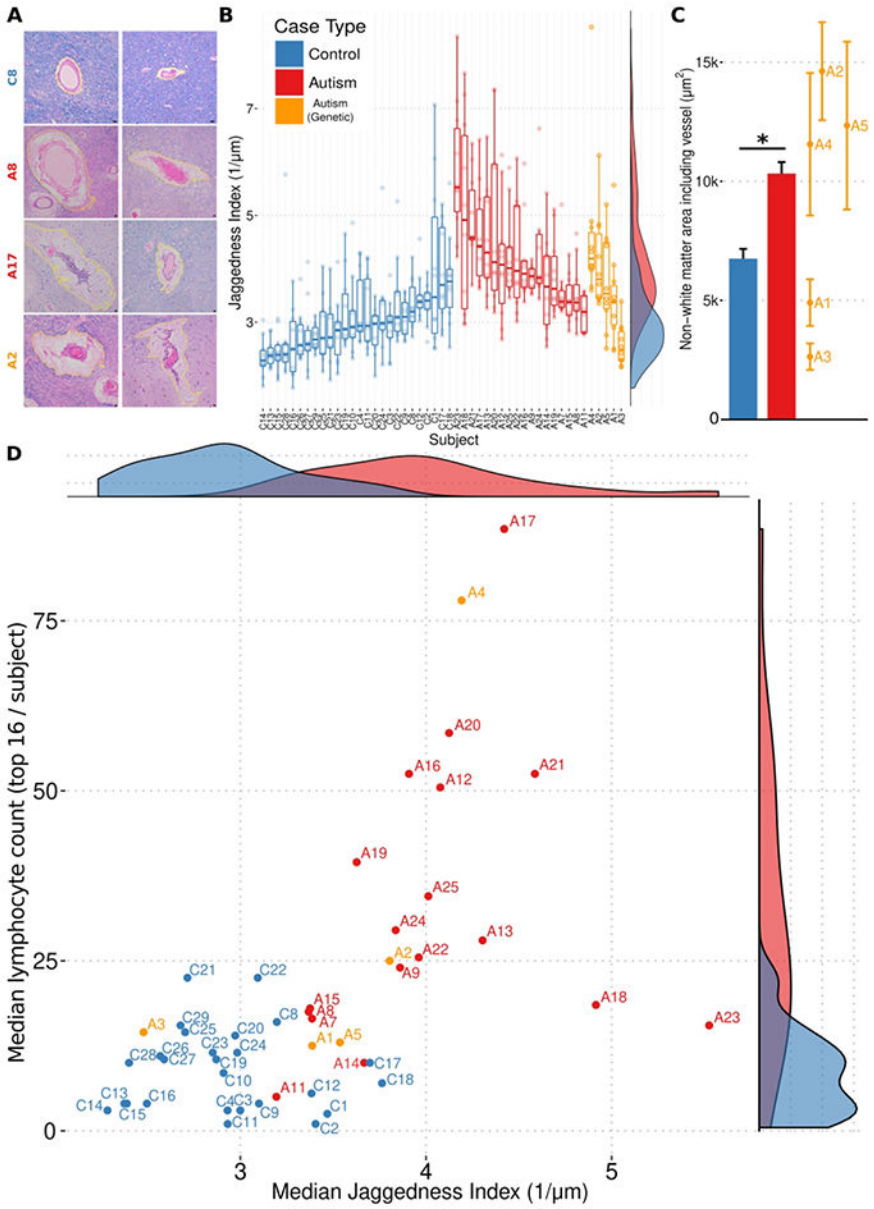

Figure 5. Increases of perivascular space (with jagged contours) and lymphocyte count separate ASD from control cases.

A gallery of photomicrographs of white matter blood vessels from a control case (A; top row), and three autism cases (A; bottom three rows) stained with H&E and LFB, with computer-assisted segmentations of perivascular area highlighted in yellow, highlights the increased perivascular area and jaggedness found in autism brain. The jaggedness index (squared second derivative of perimeter normalized to area) of the perimeters of these spaces (perivascular parenchymal contours) is plotted for each measured white matter vessel in every autism and control case (B). Dots represent jaggedness index for the area surrounding a single vessel. Overlaid box-and-whisker plots represent the medians, upper and lower quartiles, and upper/lower quartiles ±1.5*(interquartile range). Smoothed density plots for all cases are shown on right margin. X-axis labels are case names. The aggregate differences

between autism and control counts are statistically significant ($p < 0.00001$; ANOVA with Tukey's post-hoc comparison of means), as are the differences between genetic autism and control ($p = 0.00009$), and the difference between autism and genetic autism ($p = 0.002$) ($N_{vessels}$[autism] = 238, $N_{vessels}$[control] = 150, $N_{vessels}$[genetic autism] = 50). The aggregate difference between the absolute perivascular spaces measured in autism cases was higher than control cases, with individual genetic autism cases spanning the range (C). Bar heights represent means, and whiskers represent s.e.m. * = $p < 0.05$, Welch's t-test. A scatter plot of median lymphocyte count (data from Figure 3B) and median perivascular tissue damage (i.e. jaggedness; data from B) for each autism and control cases yields a clear separation (D). Marginal density plots for median lymphocyte counts and median perivascular tissue damage shown in the right and top subpanels, respectively.

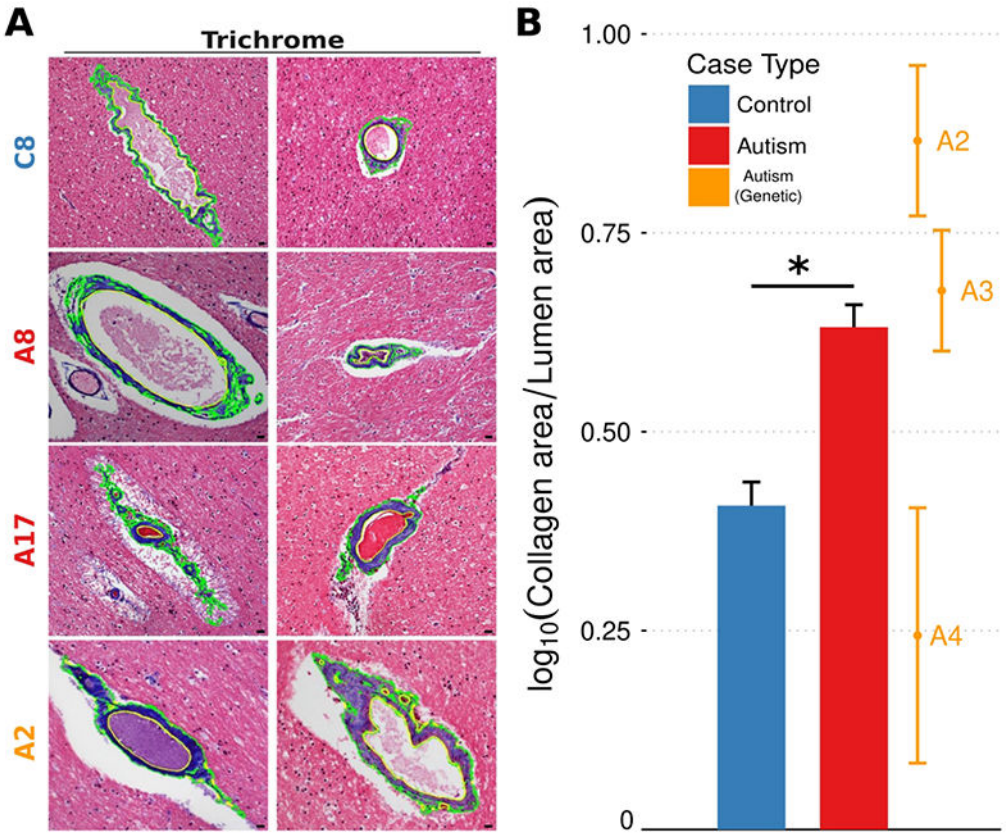

Figure 6. Increased perivascular collagen in ASD brains.

A gallery of photomicrographs of white matter blood vessels from a control case (top row), and three autism cases (bottom three rows) stained with trichrome, with computer-assisted segmentations of blue collagen highlighted in green, highlights the increased perivascular collagen found in autism cases (A). The amount of perivascular collagen in white matter for each measured vessel in every case, normalized to the area of the vessel lumen, is higher across autism cases compared to controls (B). The aggregate differences between autism and control counts are statistically significant ($p < 0.00001$; ANOVA with Tukey's post-hoc comparison of means), as are the difference between genetic autism and control ($p = 0.00003$), but not the difference between autism and genetic autism ($p = 0.88$) ($N_{vessels}$[autism] = 120, $N_{vessels}$[control] = 134, $N_{vessels}$[genetic autism] = 18).

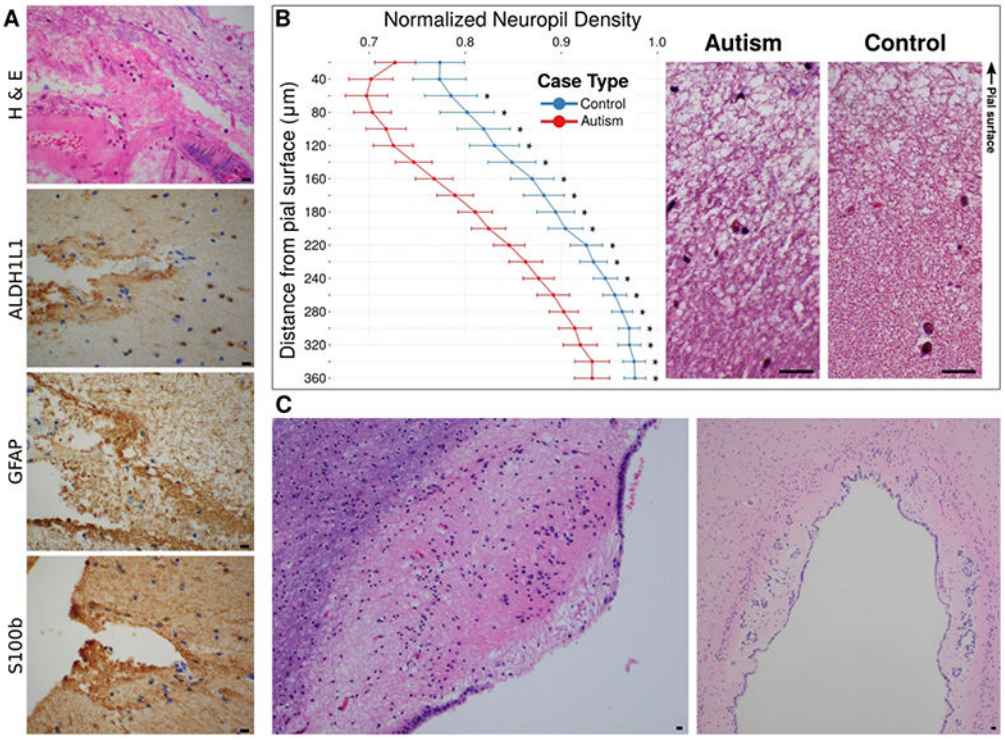

Figure 7. Rarefied cortical neuropil and leptomeningeal astroglial debris in autism.

Eosinophilic membranous debris can be seen in the leptomeningeal space between the pial surface and a leptomeningeal blood vessel (A, top; H&E). The debris stained positively on adjacent sections with antibodies to GFAP, ALDH1L1, and S100b, confirming its astroglial origin (A, bottom three panels). All scale bars represent 40 μm. Comparison of density of neuropil, excluding cell nuclei and normalized to density in an adjacent deep cortical layer on same slide, at increasing depth away from the pial surface shows rarefaction in the autism cases relative to controls (B, left). The vertical axis is aligned with the example images in the right panel. These images are co-aligned such that the junction of pia and cortex forms the top border of the images. Reductions in density are observed at depths of 60 – 360 μm in the autism cases. * = $p < 0.05$, Welch's t-test with Bonferroni correction for multiple comparisons; N_{casas}[autism] = 24, N_{casas}[control] = 23. In a subset of autism cases, the ependymal surface, another brain-CSF interface, was damaged showing granular ependymitis (C, left), and buried ependymal canals (example, cerebral aqueduct shown in C, right).

Table 1.

Study subject data.

Subject data including age, sex, autism diagnosis status, known genetic information, history of seizure or seizure disorder, unfixed brain weight, cause of death, and post-mortem interval (PMI) prior to brain fixation are compiled. Autism (susp) refers to cases for which the diagnosis of autism was made based on history, but not validated by standardized interviews with patient/family. SUDEP = sudden unexplained death in epilepsy. ARDS = acute respiratory distress syndrome. PDD = pervasive developmental delay. Genetic mutations are taken from D'Gama et al, 2015[55].

Case	ABN ID	Type	Age	Sex	Known Genetics	Hx Seizures	Brain Wt. (g)	Cause of Death	PMI (hrs)
A1	AN16641	Autism	9	M	*	Yes	1320	Possible SUDEP	27
A2	AN01570	Autism	18	F	†	Yes	2100	SUDEP	7
A3	AN00090	Autism	10	F	ǂ	Yes	1050	Drowning	17
A4	ABN_JU7U	Autism	25	M	**	Yes	1680	Possible SUDEP	23
A5	AN01678	Autism	5	M	††	Yes	1112	ARDS	16
A6	AN00581	Autism	13	M		Yes	1900	Drowning	16
A7	AN01293	Autism	9	M		No	1690	Cardiopulmonary arrest	4
A8	AN11143	Autism	14	M		Yes	1770	Complications of PDD	35
A9	AN14266	Autism (susp)	5	M		No	1420	Cardiac arrest	20
A10	AN01613	Autism	29	M		No	1800	Myocardial infarction	*Unk*
A11	AN13646	Autism	41	F		No	1190	Cancer	25
A12	AN14243	Autism	15	F		No	1130	Cardiac arrest	41
A13	AN14967	Autism	68	M		No	1205	Respiratory arrest	40
A14	AN19923	Autism	49	M		No	1390	Cancer	21
A15	AN09454	Autism	17	M		Yes	1526	Cardiac arrest	46
A16	AN09412	Autism	29	M		No	1380	Undetermined	38
A17	ABN_VPJ6	Autism	33	F		Yes	1528	Undetermined	36
A18	ABN_X5T5	Autism	37	M		Yes	1240	Undetermined	36
A19	ABN_AMF7	Autism	54	F		No	1260	Opiate overdose	51
A20	ABN_B6S3	Autism	14	M		Yes	1506	Anoxic brain injury	35
A21	ABN_Q5NC	Autism (susp)	22	M		No	1470	Suicide	36
A22	ABN_YBX7	Autism (susp)	18	M		Yes	1515	Seizure; aspiration	22
A23	ABN_3HUF	Autism	23	M		Yes	1200	Aspiration pneumonia	22

Case	ABN ID	Type	Age	Sex	Known Genetics	Hx Seizures	Brain Wt. (g)	Cause of Death	PMI (hrs)
A24	ABN_AZC6	Autism	35	M		No	1660	Cardiac arrest	38
A25	ABN_285A	Autism	8	M		No	1520	Myocarditis	23
C1	*N/A*	Control	27	M		No	1425	Liver failure	12
C2	*N/A*	Control	27	M		Yes	1630	Pulmonary hemorrhage	24
C3	*N/A*	Control	40	F		No	1120	Cancer	17
C4	*N/A*	Control	33	F		No	1550	Sepsis	18
C5	*N/A*	Control	21	M		Yes	1250	Cardiopulmonary arrest	36
C6	*N/A*	Control	46	M		Yes	1630	Status epilepticus	18
C7	*N/A*	Control	64	M		Yes	1140	Status epilepticus	30
C8	AN00404	Control	47	M		Yes	1300	Cardiac arrhythmia	19
C9	AN07591	Control	16	M		Yes	1230	Myocardial infarction	22
C10	AN01891	Control	24	M		No	*Unk*	Unknown	35
C11	AN17526	Control	39	F		No	*Unk*	Asphyxiation	25
C12	AN17139	Control	25	F		No	1450	Respiratory arrest	31
C13	ABN_N85Y	Control	50	F		No	1010	GI bleed	23
C14	ABN_G42J	Control	57	M		No	1600	Cardiac arrest	47
C15	ABN_AAJH	Control	53	F		No	1350	Myocardial infarction	19
C16	ABN_T26M	Control	57	M		No	1430	Asphyxiation	19
C17	ABN_MD2U	Control	43	F		Yes	1100	Sepsis	18
C18	ABN_82QN	Control	1	F	##	Yes	1000	Undetermined	53
C19	*N/A*	Control	17	M		No	1500	*Unknown*	10
C20	*N/A*	Control	19	M		No	1550	*Unknown*	11
C21	*N/A*	Control	2	M		No	1080	*Unknown*	24
C22	*N/A*	Control	16	M		No	1630	*Unknown*	24
C23	*N/A*	Control	20	M		No	1330	Cardiomegaly, hypertensive	15
C24	*N/A*	Control	14	M		No	1408	Drowning	25
C25	*N/A*	Control	20	M		No	1535	Gunshot wound	24
C26	*N/A*	Control	5	M		No	1300	Asphyxia	16
C27	*N/A*	Control	18	M		No	1420	Asphyxia	24
C28	*N/A*	Control	2	F		No	1000	Drowning	19

Case	ABN ID	Type	Age	Sex	Known Genetics	Hx Seizures	Brain Wt. (g)	Cause of Death	PMI (hrs)
C29	*N/A*	Control	16	F		No	1275	Gunshot wound	14
C30	*N/A*	Control	13	F			1300	Bronchial asthma	18

[*] ARID1B, CACNA1C, SLC6A8.

[†] PTEN.

[‡] Angelman's syndrome, SETD2.

[**] 47,XYY karyotype.

[††] dup15q karyotype.

[##] CDKL5.

Ann Neurol. Author manuscript; available in PMC 2020 May 09.